

A 90 GHz Bolometer Camera Detector System for the Green Bank Telescope

Dominic J. Benford¹, Mark J. Devlin², Simon R. Dicker², Christine A. Allen¹, Troy J. Ames¹, Ernest D. Buchanan^{1,3}, Tina C. Chen^{1,4}, James A. Chervenak¹, Joshua B. Forgiione¹, Kent D. Irwin⁵, Jeff Klein², Brian S. Mason⁶, S. Harvey Moseley¹, Roger D. Norrod⁶, Philip R. Jewell⁶, Johannes G. Staguhn^{1,3}, Mark P. Supanich², Edward J. Wollack¹

1 – NASA / Goddard Space Flight Center, Greenbelt, MD 20771 USA

2 – University of Pennsylvania, Philadelphia, PA 19104 USA

3 – SSAI, Lanham, MD 20706 USA

4 – GS&T, Greenbelt, MD 20770 USA

5 – NIST / Boulder, Boulder, CO 80305 USA

6 – NRAO, Green Bank, WV 24944 USA

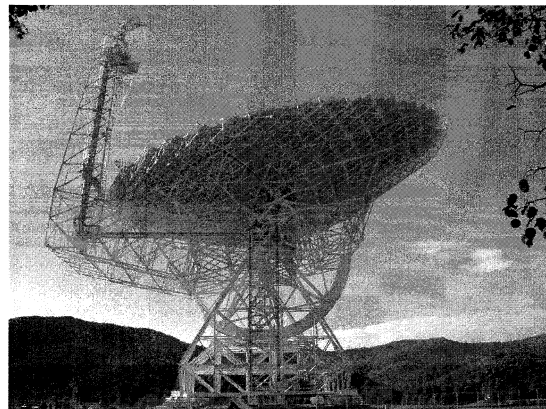
Abstract

We describe a close-packed, two-dimensional imaging detector system for operation at 90GHz (3.3mm) for the 100m Green Bank Telescope (GBT). This system will provide high sensitivity ($\sim 500\mu\text{Jy}$ in 1s) rapid imaging ($15^\circ \times 15^\circ$ to $250\mu\text{Jy}$ in 1 hr) at the world's largest steerable aperture. The heart of this camera is an 8×8 close-packed, Nyquist-sampled array of superconducting transition edge sensor (TES) bolometers. We have designed and are producing a functional superconducting bolometer array system using a monolithic planar architecture and high-speed multiplexed readout electronics. With an NEP of $\sim 2 \cdot 10^{-17}$ W/ $\sqrt{\text{Hz}}$, the TES bolometers will provide fast, linear, sensitive response for high performance imaging. The detectors are read out by an 8×8 time domain SQUID multiplexer. A digital/analog electronics system has been designed to enable read out by SQUID multiplexers. First light for this instrument on the GBT is expected within a year.

Introduction

The Green Bank Telescope (GBT; Prestage & Maddalena 2003) is an off-axis Gregorian telescope with a 100 m diameter unobstructed beam, providing a clear view of the sky from Green Bank, West Virginia (Figures 1 & 2). Designed to operate at frequencies between 290MHz and 115GHz, its surface can be actively controlled to provide an RMS surface error of around 0.21mm (although this control system is still under development). Factoring in the beam efficiency at 90GHz, the effective aperture of the GBT is around 2500m^2 , with a 90GHz beamwidth of $8.4''$.

We have undertaken to build a camera for the GBT for operation at its highest frequency of operation (90GHz, or 3.3mm). This camera will feature a close-packed detector array of 8×8 pixels, covering a field of view of $32'' \times 32''$. The camera will be optimized to obtain rapid, high-fidelity images of the sky with unprecedented sensitivity. Its mapping speed will be faster than that of previous telescopes, achieving a better sensitivity and a better angular resolution. The instrument team is led by Mark Devlin at the University of Pennsylvania, where construction of the instrument is taking place, including responsibility for the cryogenics and optics. The detectors and portions of the



Figures 1 & 2. Views of the Green Bank Telescope from above and below; the primary mirror is 100 m across.

readout electronics are provided by NASA/GSFC, while SQUID components and other readout electronics are provided by NIST/Boulder, and software is developed by the NASA/GSFC and NRAO/Green Bank.

Scientific Justification

At a wavelength of 3.3mm the dominant astrophysical sources of emission are thermal continuum emission from dust, the cosmic microwave background, and nonthermal emission.

One of the key science projects for a 90GHz camera of such high sensitivity and angular resolution will be to conduct a deep survey of distant galaxies. At cosmological distances, the dust emission in the submillimeter will be redshifted towards millimeter wavelengths. This observed 90GHz flux is thus emitted at higher frequencies, and so the steeply rising spectrum of such emission means that galaxies do not become substantially fainter as they are seen at greater distances. This “negative K correction” implies that a deep survey at 90GHz would find galaxies at all redshifts equally well (Blain et al. 1999), as shown in Figure 3. As a result, the number of sources detected at 90GHz can be very large... tens of thousands per square degree (Figure 4). An example of what such a survey would look like is shown in Figure 5. This simulation shows the high detection capability of this camera.

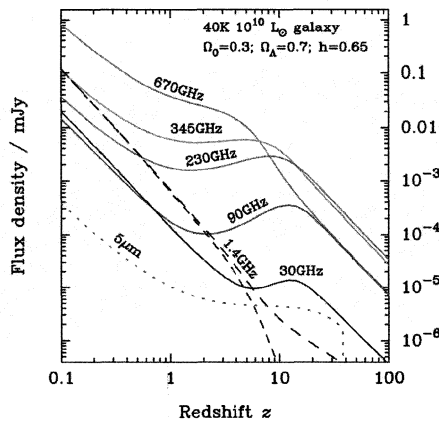


Figure 3. Redshifted flux densities (Blain et al. 2002).

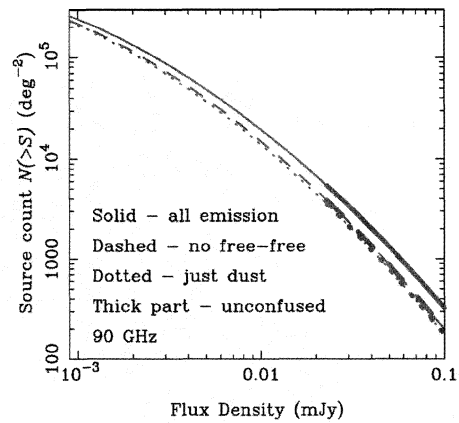


Figure 4. Galaxy counts at 90GHz (Blain 2004).

The power of a 100m telescope with an imaging array will produce a potent mapper of the Sunyaev-Zeldovich effect. For example, the Nobeyama 45m telescope operating at 21GHz can map to 500μJy in 34 hours with an 80” beam (similar to cluster angular size); the GBT operating at 90GHz will map at 8” resolution to 50μJy in 15 minutes. In addition to cosmological studies, nearby star and planet formation regions will be opened up for study by the GBT with its 90GHz camera. It can see the very faint emission from cold dust around protostars with unprecedented sensitivity and angular resolution.

Instrument Description

We are building the Penn Array Receiver (PAR), the first-generation 90GHz camera for the GBT. The detector system for the PAR is a superconducting transition edge sensor (TES) bolometer array and readout electronics providing 64 pixels in a close-packed 8x8 format. Compact on-axis reimaging optics provide a 32”x32” image on the sky and an operating wavelength of 3.3mm, where the diffraction-limited beamwidth is 8”. The detectors are read out by a super-conducting quantum interference device (SQUID) amplifier produced at NIST/Boulder and high performance electronics developed at NASA/GSFC and NIST/Boulder. The

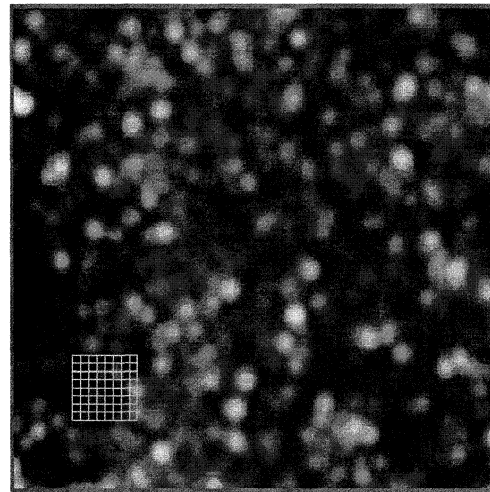


Figure 5. Simulated image of the sky showing the distribution of galaxies seen by the GBT at 90GHz.

software for controlling the PAR and for reducing the data is being produced by a combination of U.Penn, NASA/GSFC, and NRAO/GB efforts, based on the Instrument Remote Control architecture (Ames 2004).

Cryogenics

The PAR requires a cryogen-free cooling system to provide refrigeration of the optics to $\sim 3\text{K}$ and the detectors to $\sim 300\text{mK}$, while inducing a minimum of vibration and operating in non-vertical orientations. The requirements on the PAR cryogenic system are several:

- The system must provide cooling of the optics to $\leq 3\text{K}$ without the use of liquid helium. Estimated load at 3K is $<100\text{mW}$ with an intermediate cooling of $<4\text{W}$ at 40K .
- $15\mu\text{W}$ of cooling at temperatures below 290mK : This must be maintained at angles of at least 57° from the vertical (corresponding to observations 20° above the horizon).
- When the receiver is not in use it may be tipped by up to 72° in any direction. After this it must be ready to use within 90min of being returned upright.
- A minimum hold time at $<290\text{mK}$ of 24h (to allow deep observations), with a goal of 68h (to allow for flexible scheduling of the telescope) is required.
- The receiver must be easily operated remotely by members of the astronomical community who are not familiar with cryogenics.
- So as not to affect the bolometers, low mechanical vibration and moderate temperature stability are needed.

Due to the remote operation requirement, expendable liquid cryogenics were ruled out. A cryostat has been designed using two multi-stage closed-cycle coolers providing several stages of cooling between 300K and 300mK . This cryostat is shown at right in Figure 6.

The $300\text{K} \rightarrow 3\text{K}$ cooling is realized by means of a commercially available pulse tube cooler (Cryomech Inc.). This cooler can provide a cooling power of 150mW at 3K and 5W at 40K . It has no moving parts at the cold end, and so is a low-vibration mechanical cooler option. Its mean time between servicing of 20kh is well suited to operation at the remote instrument chamber of the GBT. Under expected parasitic loading, the temperatures of the two stages will be around 40.5K and 2.7K . The only difficulty with this cooler is that it is orientation-dependent: the cooling power at fixed temperature can drop by a factor of two when tilted to 30° off of vertical. Tipping the system to 57° from the vertical resulted in the first stage warming up to 70K in 2h . The second stage was relatively unaffected, showing only a rapid warming to 3.4K before becoming stable. Tests of the cooler indicated that the temperature of the first stage under constant load changes dramatically but transiently when the cold head is tilted. For tilts of $\Delta \sim 40^\circ$, a transient of around 2K occurs with a settling time of perhaps half an hour; similar transients of $\sim 6\text{K}$ occur for larger ($\Delta \sim 80^\circ$) tilts.

Closed cycled cooling to 250mK

We use the two-stage pulse tube cryocooler to cool the condenser of a ^4He sorption refrigerator, which is in turn used to cool the condenser of a ^3He sorption refrigerator (Figure 7; Devlin et al. 2004). This system has nominal temperatures of 40.5K (pulse tube first stage), 2.7K (pulse tube second stage), 0.7K (^4He refrigerator) and 0.250K (^3He refrigerator—unloaded). With a load of $15\mu\text{W}$ the ^3He refrigerator runs at 270mK and has a hold time of 72.7h . This temperature was stable to 0.09mK on timescales from 1s to 10min . After initial cooling, long-term drifts dropped below 0.2mK/h , and the refrigerator RMS temperature noise is $90\mu\text{K}$ at a timescale of one minute.

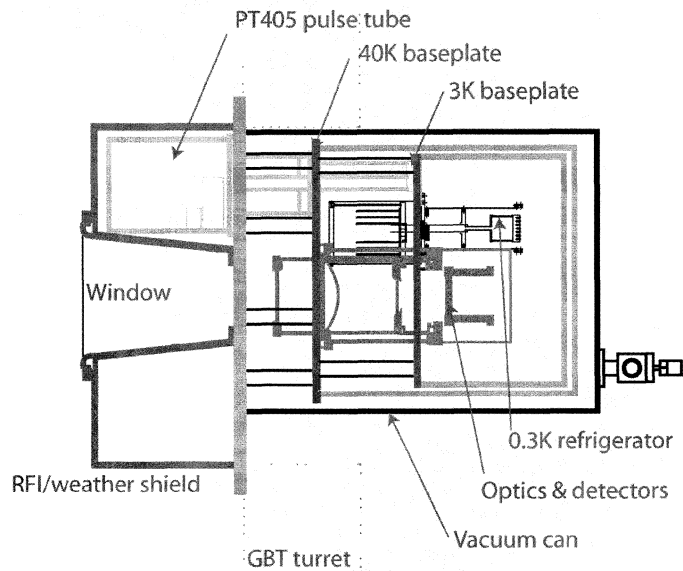


Figure 6. Side view of cryostat design; light enters from left.

The cycling of the refrigerators is computer controlled, occurring on demand or autonomously when the ^3He refrigerator runs out. Typically it takes 4.5 h from the start of a cycle to when the ^3He refrigerator is stable below 290 mK. The cycling time is dominated by the limited cooling power of the pulse tube. Cycling has been shown to be effective at tilts up to at least 45° from the vertical.

The pulse tube is designed to operate vertically, whereas the sorption coolers are designed to be relatively orientation-insensitive. When tilted to 57° off of vertical the ^3He stage is unaffected, while the ^4He stage warms up by 10mK. On tilting the system to 72° the second stage of the pulse tube warms to 20 K in an hour and the charcoal pumps stop working, but the system then recovers within 40 min of being returned to vertical. With this last test we were able to conclude that the cryogenic system would meet all the above requirements on the GBT.

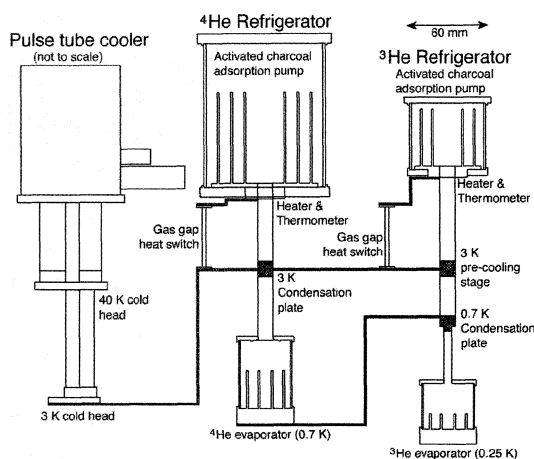


Figure 7. Diagram illustrating the thermal connections of the $^4\text{He}/^3\text{He}$ refrigerator.

Optics

Previous feedhorn-coupled bolometer arrays such as SCUBA (Holland et al. 1999) have had beams spaced by two resolution elements ($2f\lambda$) on the sky. Due to $1/f$ noise, missing data must be filled in as quickly as possible using complex scan strategies. This is often accomplished using the secondary or tertiary optics of a telescope to chop the beams on the sky. While this does reduce the influence of slow drifts on the final map, the fidelity of the image is compromised by the fact the chopping is an inherently differential technique. In the case of a large map of isolated sources, the result is an accurate map, but with additional noise arising from the differenced measurement. In the case of extended sources, the map is often inaccurate as well. The SHARC II instrument on the Caltech Submillimeter Observatory (Staguhn et al. 2003) has recently yielded excellent imaging quality without the use of a chopped measurement, by means of redundant sampling.

There is no easy fast way to chop the GBT. By using a fully sampled array with pixels spaced by $0.5f\lambda$ on the sky, maps can be made in a single scan and no fast chopping is needed. To get beams this close, feedhorns cannot be used above our array. We also note that 90 GHz feedhorns are expensive and difficult to manufacture. Reimaging with mirrors requires large volumes and a difficult alignment process. Lenses are compact and yield good off-axis image quality, and so are a good choice. However, they require good anti-reflective coatings and careful design to reduce ghosting.

Instead, illumination of the detectors is controlled using two aspheric silicon lenses with a cold Lyot stop between them (Figure 8). The bandpass is defined using reflecting capacitive mesh filters from U. Cardiff. The Lyot stop controls stray light and, along with filter 3, it limits the amount of power incident on each detector. Everything inside the Lyot stop is cooled to either 2.7 or 0.270 K. Power landing on the detectors comes from two main directions; through the Lyot stop (which is a sum of emission from the telescope, the atmosphere and the astronomical signal) and the 2.7 K structure around the Lyot stop (which is reduced to acceptable levels by bandpass filter 3). When all sources of power are considered, the telescope's optics (warm and cold) will contribute 0.7 pW per detector. The atmosphere should contribute 0.5–2.8 pW (depending on atmospheric opacity and telescope elevation) to give a total of 1.2–3.5 pW. Given the low intrinsic noise from the detectors, the receiver noise should be limited by the atmosphere to $1.2 \times 10^{-17} \text{ W}/\sqrt{\text{Hz}}$, corresponding to a sensitivity on astronomical sources of 500–730 $\mu\text{Jy}\cdot\sqrt{\text{s}}/\text{detector}$.

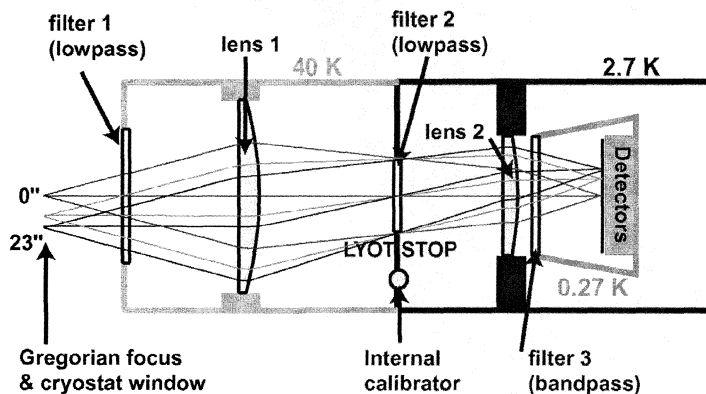


Figure 8. Optical design of the PAR.

Detector Array

The detector array format is chosen to be an 8x8 pixel array with a pitch of 3.3mm (chosen to be the wavelength). The power from the atmosphere sets the saturation power of the detectors to 12pW. The operating temperature will be around 450mK, which then limits the detector NEP to $2 \cdot 10^{-17}$ W/ $\sqrt{\text{Hz}}$. The detectors are planar silicon membrane bolometers, each with a superconducting transition edge sensor (TES) of a Mo/Au bilayer (Benford et al. 1999).

From the ground, the atmosphere is the only important source of background power on the bolometers. Figure 9 shows the expected atmospheric emissivity (Grossman 1989) for the site of the GBT at left; this can be converted into an atmospheric photon noise equivalent power (NEP), as shown at right. The PAR detectors will need to achieve a phonon and Johnson noise sum of $<4 \cdot 10^{-17}$ W/ $\sqrt{\text{Hz}}$ in order to be background-limited, and must be able to absorb up to ~ 8 pW in order to avoid saturation (a conservative value, since the actual power will be known only after engineering observations). This puts a stiff requirement on the dynamic range of the bolometers: the ratio of maximum power detected to the minimum power detectable in unity bandwidth is over 10^5 .

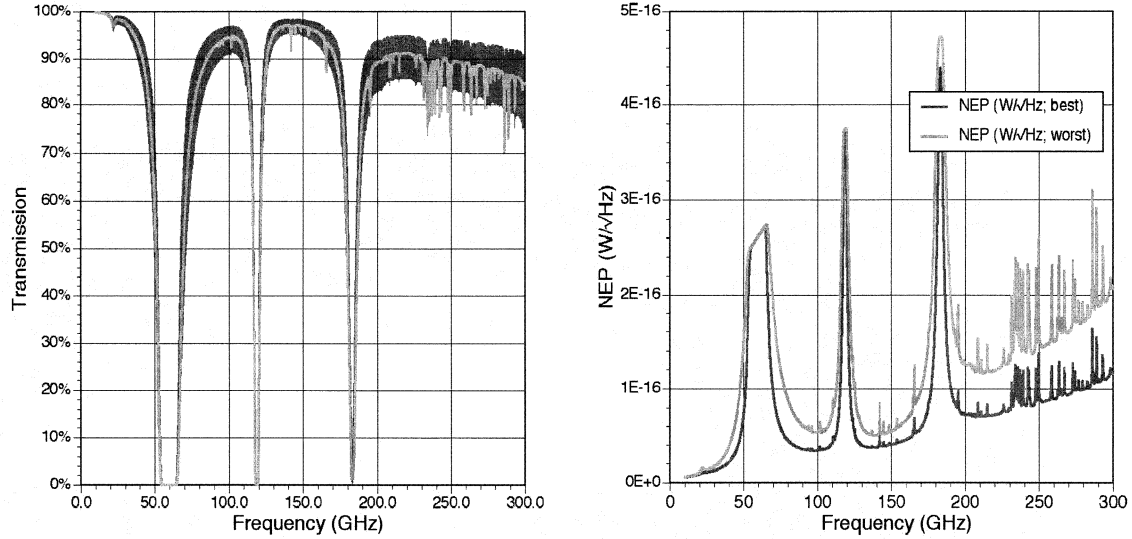


Figure 9. (Left) Atmospheric transmission and (Right) NEP for representative ranges of West Virginia weather.

In order to satisfy this requirement, a TES is used to read out the detector temperature. A TES bolometer has a faster response time than an identically designed, same-sensitivity semiconducting bolometer (or a more sensitive bolometer for the same response time) due to the strong negative electrothermal feedback intrinsic in a voltage-biased TES (Irwin 1995). TES bolometers are inherently low impedance devices, so they are well-matched to being read out by DC SQUID amplifiers (Welty & Martinis 1993). These amplifiers have a large noise margin over the bolometer noise. This permits the bolometer to be read out in a multiplexed fashion by a suitable SQUID multiplexer (Chervenak et al. 1999), reducing the amplifier size and wire count. Because SQUID amplifiers operate at the base temperature of the bolometer, they can be coupled very closely, removing the complex mechanical-thermal interfaces necessary with semiconducting bolometers.

A TES bolometer is fundamentally no different from a semiconducting bolometer, other than a change in the thermistor that has substantial implications. Infrared light is absorbed in the bolometer and converted into heat which warms the detector of heat capacity C above its nominal temperature T_{bias} (Figure 10). This temperature change is converted into a resistance change which is measured electrically. The heat is conducted away through a thermal conductance G to a heat sink at T_{bath} . A superconducting transition at temperature T_C yields an extremely sharp but continuous change in resistance from near zero to the normal state resistance (Figure 11). A unitless measure of the sharpness of the transition is defined as the sensitivity α :

$$\alpha \equiv \frac{d \log R}{d \log T} = \frac{T}{R} \frac{dR}{dT} \approx \frac{2T_C}{\Delta T}$$

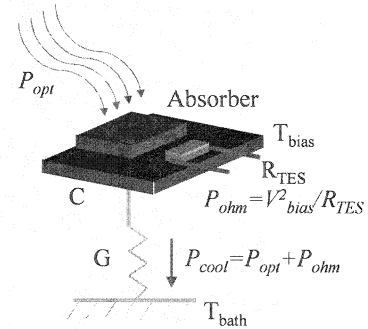


Figure 10. Schematic of the operation of a TES bolometer.

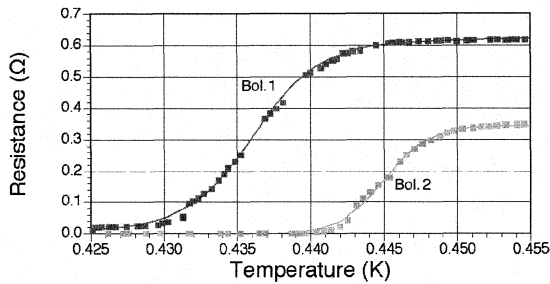


Figure 11. R_{TES} vs. T_{bias} for representative bolometers.

through the action of the electrothermal feedback by a factor of $(n/\alpha)^2$. The end result of this is that the intrinsic noise of a TES bolometer is typically dominated by the phonon noise alone.

One downside of TES bolometers is that, above some optical loading, the superconductor is driven normal and the detector responsivity goes to zero. This poses an interesting fundamental limit. The saturation power of a superconducting bolometer is $P_{sat} \approx GT_C/\eta$, where G is the thermal conductivity and $\eta \sim 5$. The phonon noise is given by $NEP_{phonon} = (4kT^2G)^{1/2}$. The photon noise is given by $NEP_{photon} = (\zeta^2 P h \nu)^{1/2}$, where $\zeta \sim 2$ when photon bunching is significant. Assuming operation at $T = T_C$ and $P = P_{sat}$, we can rearrange to find that photon and phonon noise are equal when $T_C = (\zeta h \nu / 2k\eta)$. At 90GHz, this point is at $T_C = 860mK$. The ratio of noise scales as $T_C^{1/2}$, so operating well below this point is necessary.

Superconducting transitions can be made in several ways. In order to produce a thermistor with a tunable T_C and with a known resistance, we manufacture superconducting-normal bilayers. The superconductor, in this case a thin film of molybdenum, has its transition temperature reduced by proximity to a thin film of a normal metal such as gold. This process is described more fully by Chervenak et al. (2003) and Allen et al. (2003). The thermistor is manufactured by deposition and photoetching to produce a small ($50\mu m \times 100\mu m \times 0.1\mu m$) active volume. Such a thermistor is shown in Figure 12.

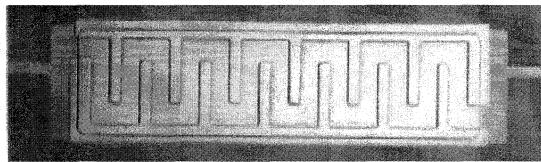


Figure 12. TES bilayer with lateral noise-suppression bars.

The voltage-current characteristic of a TES bolometer is quite different from that of a semiconducting bolometer. If we consider a voltage-biased TES cooling down from the normal state, the device exhibits a constant resistance ($I = V/R$). If we lower the bias voltage, at some point the bias power becomes too little to keep the device in the normal state, and it will begin to drop in resistance. Because the transition width is small, the TES is nearly isothermal at any point on the transition, and so the total dissipated power must be constant. In this case, the current becomes a hyperbolic function of the voltage, $I = P/V$. At some point, the bias current reaches a maximum value (set by electronics) and the TES becomes superconducting. The responsivity of a TES on its transition is approximately $1/V$ (A/W).

The function of a SQUID readout is more complex than of a FET, due to the fact that a SQUID's output is a periodic rather than linear function of the input. A SQUID transduces a measurement of magnetic flux into a voltage with extreme sensitivity. We use a voltage-biased TES sensor, so that the current varies as the resistance changes. This current couples through an inductor into the SQUID, which produces a voltage that is periodic in the input current. We then place a second inductor, called the feedback coil, next to the SQUID, and introduce a current exactly opposite the measured current in the input coil. As the input coil current changes (i.e., as the TES resistance changes), the SQUID reads a differential current. The feedback current is changed based on this difference to result in a nulled flux through the SQUID. The SQUID output is now a linearized function of the input, and the feedback current is always equal to the current through the TES.

A crucial element in the design of a large-format array is the multiplexer. As a collaborative effort between NASA-Goddard and NIST-Boulder we have, over the past few years, made substantial progress in the use of SQUID multiplexers for the readout of low-impedance devices. An eight-input SQUID multiplexer/amplifier (Chervenak et al. 1999) has been used to demonstrate Johnson-noise-limited readout (Staguhn et al. 2001), detection of infrared light with TES bolometers (Benford et al. 2000), and operation in an astronomical application (Benford et al. 2001). There is now a 32-input SQUID multiplexer with a more advanced architecture (Irwin et al. 2001), shown below in Figure 13. This multiplexer operates using time-domain multiplexing, and can operate at rapid switching rates with

low channel-to-channel crosstalk. A second stage SQUID amplifier is included on this chip to provide sufficient output to drive the multiplexed signal to a SQUID amplifier located elsewhere.

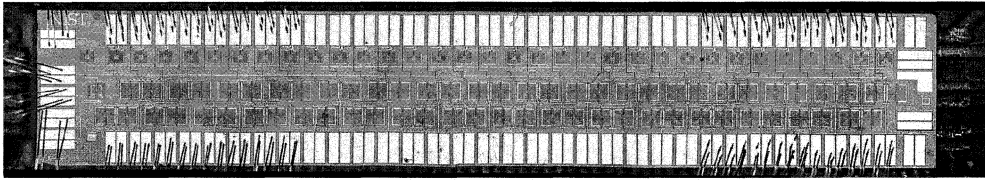


Figure 13. 32-input SQUID multiplexer chip manufactured at NIST-Boulder.

In the case of a multiplexed SQUID readout, several inputs are read through one output. Under control by a computer, a given input SQUID is turned on and its differential current (the signal minus the feedback) is read out. This difference current is then nulled by changing the feedback current, and its value – equal and opposite to the TES current – is stored for the future. The next SQUID is read out similarly, until all inputs have been read. On the next cycle, the previous readout of the TES current is looked up from memory, and its current is nulled with the previous feedback value. The SQUID then reads out the difference between the previous reading and the present reading, providing a linearized response. There is a flexible, compact, and modular analog / digital data acquisition subsystem to control and read out this complex but capable multiplexed amplifier array (Benford et al. 2003; Reintsema et al. 2003; Forcione et al. 2004).

The mechanical design for the detectors uses a 3.3mm-pitch, planar silicon membrane, 1 μ m thick, suspended by low thermal conductance legs. This is shown in Figure 14. The pitch was chosen to permit absorbers of $\sim\lambda$ in size, permitting the use of a filled-sheet absorber rather than an antenna.

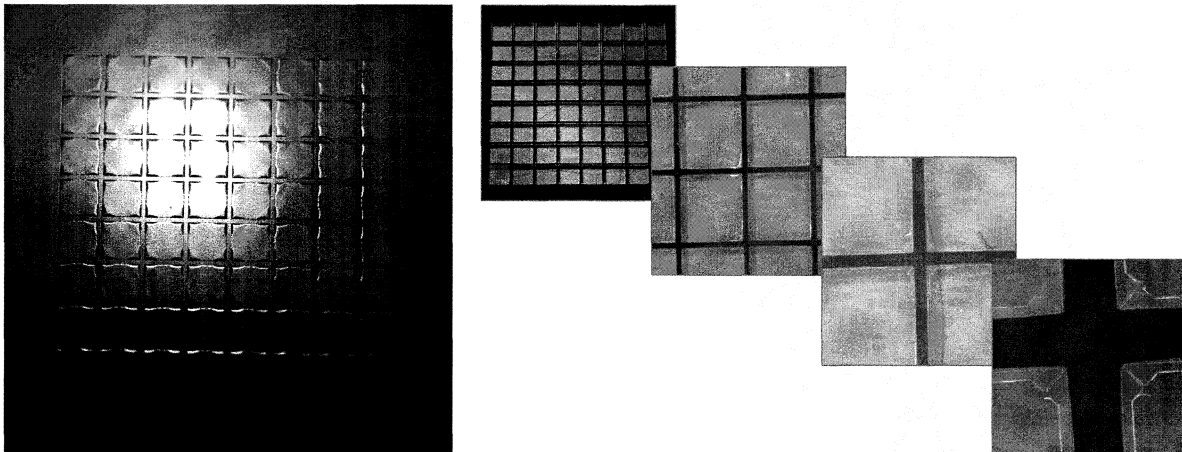


Figure 14. Mechanical model of the PAR 8x8 bolometer array, showing the overall design and the details of the thermal attachment of the membrane at the corner.

Detector Characterization

The PAR bolometers are in a development stage where variations of the bolometers are being characterized. The results presented here are taken from samples of 1x8 arrays consisting of 1mm² pixels. More detailed discussions of these detectors are presented elsewhere by Staguhn et al. (2004). The dark noise is within a factor of <2 of the theoretical prediction of 10⁻¹⁷ W/ \sqrt Hz, the dynamic range is around a factor of 5 \cdot 10⁵, and the time constant is 1ms.

In Figure 15, we show the calibrated current vs. voltage for a set of detectors taken on several multiplexed bolometers simultaneously. The normal portion of the curve is a straight line, becoming hyperbolic at lower bias voltages as the detector resistance drops down the superconducting transition curve. At right in Figure 16, we show the response of several detectors to a blackbody source of known temperature. The response is calibrated by a multiplicative factor to account for the unknown coupling to the source. Over a range of three octaves in optical loading, the bolometers respond similarly to their predicted behavior.

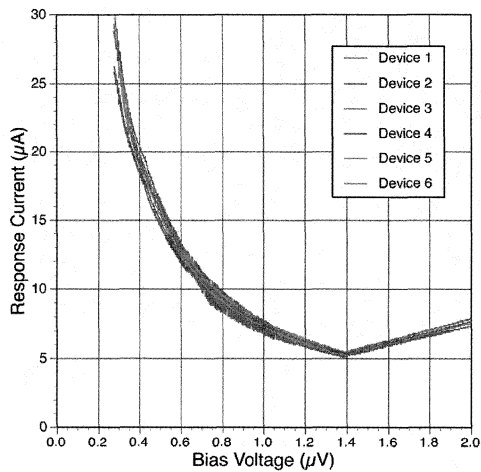


Figure 15. Current vs. voltage for several bolometers.

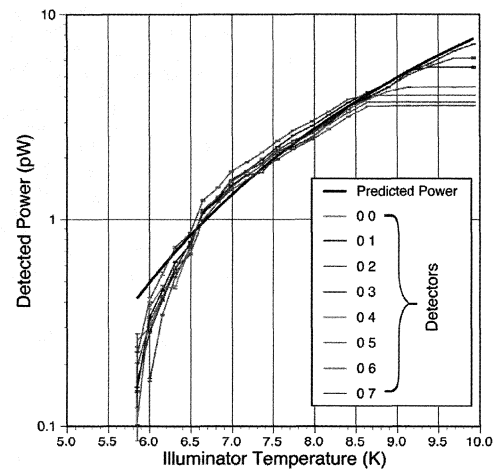


Figure 16. Optical response to blackbody illumination.

References

- R.M. Prestage & R. Maddalena, "Green Bank Telescope: Status and Early Results", Proc. SPIE #4837, pp. 944-953 (2003).
- A.W. Blain, I. Smail, R.J. Ivison & J.-P. Kneib, "The History of Star Formation in Dusty Galaxies", MNRAS 302, pp. 632-648 (1999).
- A.W. Blain, I. Smail, R.J. Ivison, J.-P. Kneib & D.T. Frayer, "Submillimeter Galaxies", Phys. Reports 369, pp. 111-176 (2002).
- A.W. Blain, private communication (2004).
- T.J. Ames, "XML in an Adaptive Framework for Instrument Control", Proc. 2004 IEEE Aerospace Conference, in press (2004).
- Cryomech Inc., PT-405; Falso Drive, Syracuse, NY 13211 USA; 1-315-455-2555.
- M.J. Devlin, S.R. Dicker, J. Klein & M.P. Supanich, "A High Capacity Completely Closed-Cycle 250mK ³He Refrigeration System Based on a Pulse Tube Cooler", Cryogenics, in press (2004).
- W.S. Holland et al., "SCUBA: A Common-User Submillimeter Camera Operating on the James Clerk Maxwell Telescope", MNRAS 303, pp. 659-672 (1999).
- J.G. Staguhn, D.J. Benford, S.H. Moseley & C.D. Dowell, "Astronomical Results from SHARC-II", NIMPR-A 520, pp. 384-386 (2003).
- D.J. Benford et al., "Superconducting Bolometer Arrays for Submillimeter Astronomy", ASP Conference series #217, "Imaging at Radio through Submillimeter Wavelengths", pp. 134-139 (1999).
- E.N. Grossman, "AT-Atmospheric Transmission Software User's Manual, v1.5", Airhead Software, 2069 Bluff St, Boulder, CO 80302 (1989).
- K.D. Irwin, "An Application of Electrothermal Feedback for High Resolution Cryogenic Particle Detection", Appl. Phys. Lett. 66 (15), pp. 1998-2000, (1995).
- R.P. Welty & J.M. Martinis, "Two-Stage Integrated SQUID Amplifier with Series Array Output", IEEE Trans. on Applied Superconductivity 3 (1), pp. 2605-2608, (1993).
- J.A. Chervenak, K.D. Irwin, E.N. Grossman, J.M. Martinis, C.D. Reintsema & M.E. Huber, "Superconducting Multiplexer for Arrays of Transition Edge Sensors", Appl. Phys. Lett. 74 (26), pp. 4043-4045, (1999).
- J.A. Chervenak et al., "Fabrication of Transition Edge Sensor X-ray Microcalorimeters for Constellation-X", NIMPR-A 520, pp. 460-462 (2003).
- C.A. Allen et al., "A Dry-Etch Process for Low Temperature Superconducting Transition Edge Sensors for Far Infrared Bolometer Arrays", Low Temperature Detectors #10, Elsevier, in press (2003).
- J.G. Staguhn et al., "TES Detector Noise Limited Readout Using SQUID Multiplexers", AIP-CP #605, Low Temperature Detectors, pp. 321-324 (2001).
- D.J. Benford et al., "Multiplexed Readout of Superconducting Bolometers", IJIMW 21 (12), pp. 1909-1916 (2000).
- D.J. Benford et al., "First Astronomical Use of Multiplexed Transition Edge Bolometers", AIP-CP #605, Low Temperature Detectors, pp. 589-592 (2001).
- Irwin, K.D. et al., "Time-Division SQUID Multiplexers", AIP-CP #605, "Low Temperature Detectors", pp. 301-304, (2001).
- D.J. Benford, G.M. Voellmer, J.A. Chervenak, K.D. Irwin, S.H. Moseley, R.A. Shafer & J.G. Staguhn, "Design and Fabrication of Two-Dimensional Superconducting Bolometer Array for SAFIRE", Proc. SPIE #4857, pp. 125-135 (2002).
- J. Forgiione, D.J. Benford, E.D. Buchanan, S.H. Moseley, J. Rebar & R.A. Shafer, "Enhancements to a Superconducting Quantum Interference Device (SQUID) Multiplexer Readout and Control System", Proc. SPIE #5498, submitted (2004).
- C.D. Reintsema et al., "Prototype System for Superconducting Quantum Interference Device Multiplexing of Large-Format Transition-Edge Sensor Arrays", Rev. Sci. Inst. 74 (10), pp. 4500-4508 (2003).
- J.G. Staguhn, D.J. Benford, S.H. Moseley, C.A. Allen, T.A. Stevenson & W.-T. Hsieh, "A Comparison of Device Characteristics of Mo/Au TES Bolometers with Different Normal Metal Bar Geometries", Proc. 15th Int. Symp. Space THz Tech., in press (2004).